Geometry of the Ag{001}-$c(2\times2)$Cl structure as determined by He diffraction

M. J. Cardillo, G. E. Becker, D. R. Hamann, J. A. Serri, L. Whitman,* and L. F. Mattheiss
Bell Laboratories, Murray Hill, New Jersey 07974
(Received 5 November 1982)

The structure of the Ag{001}-$c(2\times2)$Cl surface has been studied with He-atom diffraction. Two proposed Cl binding geometries have been considered as structural alternatives: the fourfold-hollow simple overlayer model and a mixed layer of coplanar Ag and Cl. We have calculated the repulsive He potential, based on self-consistent charge densities of the target, for both configurations. The two geometries are easily distinguished. The charge densities for the overlayer structure yield a corrugation which is in good agreement with the scattering data and lead to an unambiguous selection between the two structural models. We have further examined the possibility that the Cl overlayer undergoes a structural phase transition or irreversibly disorders at elevated temperatures. We find no change in the structure for temperatures up to 650 K, at which point Cl leaves the surface.

I. INTRODUCTION

We present a He diffraction study of the binding geometry of adsorbed Cl on the Ag{001} surface which forms a $c(2\times2)$ periodic array. Cl adsorption on this surface was the subject of a low-energy electron diffraction (LEED) structural investigation[1] in which it was concluded that the Cl occupies the fourfold-hollow sites above the Ag surface. This simple overlayer model (SOM) is illustrated in Fig. 1(a). An alternative geometry considered in the LEED investigation is the mixed layer model (MLM), which consists of the Cl atom occupying substitutional positions on the silver surface suggesting a monolayer of epitaxial silver chloride, Fig. 1(b). In the LEED study the MLM yielded comparable agreement to the SOM for a large number of diffracted beams. However, on the basis of selected key features in the intensity-voltage (I-V) spectra for four particular beams the SOM was preferred. For the SOM the LEED study indicated a vertical distance of the Cl nucleus above the Ag{001} plane, $d_z=1.57-1.75$ Å. Subsequent to the LEED work, the $c(2\times2)$Cl system was studied with ultraviolet photoemission spectroscopy[2] and changes in the electron binding-energy spectra associated with the Cl adsorption were identified. This stimulated a theoretical investigation of the Ag—Cl bonding on this surface based on self-consistent electronic structure calculations.[3] Comparing the Cl local density of states (LDOS) with the photoemission difference spectra showed qualitative discrepancies. Calculations for both the MLM and SOM geometries demonstrated that the key features of the photoemission difference spectra were considerably closer to the LDOS calculated for the MLM than the SOM. With consideration of the nearly comparable level of agreement with LEED data for both models, the suggestion was made that the MLM might indeed be the favored structure.

There are also the possibilities that two different ordered structures of the same symmetry can be formed or that the ordered $c(2\times2)$ undergoes a disordering transition (reaction) at elevated temperatures. A surface phase transition was recently suggested by Kitson and Lambert[4] based on the observation of a strong increase in the

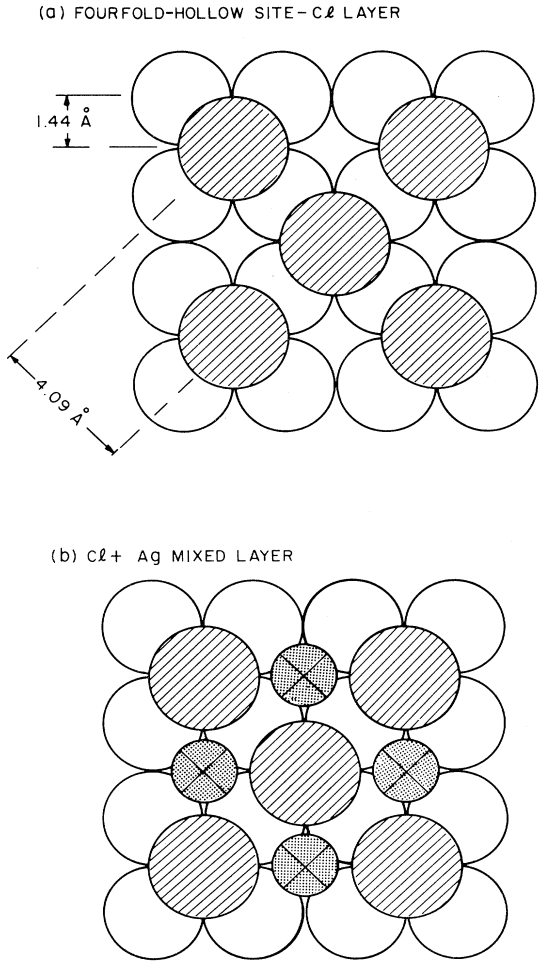

FIG. 1. (a) Model of the simple overlayer of Cl on Ag{001}. (b) Model of the mixed layer of Cl and Ag, with mixed layer Ag "ions" drawn smaller than surface Ag atoms.

electron-stimulated desorption (ESD) cross section accompanied by an irreversible deterioration of the $c(2\times2)$ LEED pattern at temperatures above 500 K.

A. He diffraction and surface charge densities

Recent developments in the description of the He-surface potential, based on the electron charge densities of the target,[5–7] and in the theory and computation of He diffraction patterns,[6] have made possible a direct and nearly first-principles connection between He diffraction and the nuclear positions of surface atoms. It has been demonstrated that the He-surface potential retains considerable sensitivity to nuclear positions if a substantial corrugation in the surface charge density extends out to the He distance of closest approach.[7] The relation between the He-surface repulsive potential and the surface electron density is based on calculating the energy of embedding He in a uniform electron gas, and neglecting the variation of the actual surface charge density across the very small volume of the He atom. In the energy range of interest, this yields a linear relationship, $V_{\mathrm{He}}(x)=A\rho(x)$. For V in eV and ρ in atomic units, $A=750$ or 670, depending on the method of calculation.[5,6] The He energies used in these experiments range from 25 to 63 meV, so the classical turning points occur at densities between approximately 3.5×10^{-5} and 9×10^{-5} a.u. These extremely low densities will typically occur 3 to 4 Å outside the surface-atom plane.

The most accurate method to find the electron charge density of a surface is to carry out a self-consistent calculation of the electron states. This can be done for an extended surface using the local-density-functional formalism[8] to treat the exchange and correlation potential. While this is the only necessary physical approximation, various mathematical approximations are made in implementing such a calculation. The first study of the electronic structure of the Ag{001}$c(2\times2)$Cl system[3] used a linear combination of atomic orbitals (LCAO) method to represent the wave functions. This formulation does not give the charge density in the far-surface region probed by the He with sufficient accuracy to permit the use of these results. These calculations were repeated using the surface linear augmented-plane-wave (SLAPW) method, and the results for the electronic densities of states were in excellent agreement with the LCAO results.[9] The SLAPW method uses numerical wave functions in the surface region,[10] and is capable of more accurate charge densities. Charge densities based on similar calculations have been successfully compared with He diffraction results for GaAs{110} and Ni{110}-(2×1)H.[7]

Charge densities based on the SLAPW calculations reported in Ref. 9 are shown in Fig. 2 for the SOM and the MLM. These figures show contours of constant charge density in a plane normal to the surface and passing vertically through the second-neighbor surface Cl in Fig. 1(a), or the Cl and Ag in Fig. 1(b). The Ag atoms at the bottom of the plots are in the second bulk layer. The Ag atoms in the last complete Ag layer in Fig. 1 lie out of the plotting plane. The contours at 4.6×10^{-5} and 10^{-4} can be regarded as, in effect, the "corrugated hard walls" for

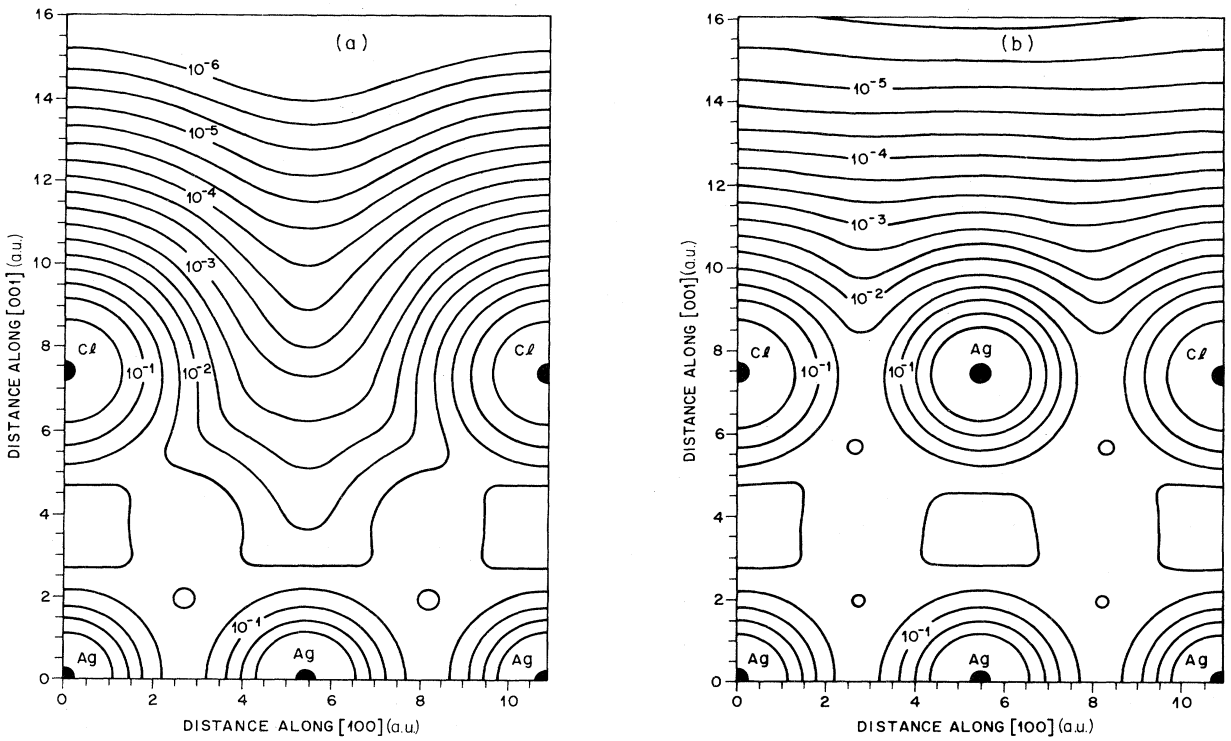

FIG. 2. (a) Valence-charge-density contours for the SOM based on SLAPW calculations. Units are electrons per a.u.^{3}, and the contour progression is 1,2.2,4.6. (b) Valence-charge-density contours for the MLM based on SLAPW calculations.

25- and 63-meV He atoms. The plotting plane has been chosen to show the maximum corrugation amplitude for the SOM, which is 2 a.u. (1 Å) peak to peak. The contrast posed by the MLM is extreme, with 0.1-Å corrugations. This is not an obvious result. The mixed layer Ag is partially ionized,[3] and might have been much less effective in "filling the hole" in the SOM charge density. The MLM geometry used here assumed coplanar Cl and Ag. Variations of the geometry away from coplanarity could induce some additional corrugation in the outer contours, but it is clear that no reasonable MLM geometry can fail to be easily distinguishable from the SOM in its He diffraction potential.

A good approximation to the repulsive He potential in the region of interest is the corrugated exponential wall model,

$$V(x)=V_0\exp\{[z-h(x,y)]/l\}\ , \tag{1}$$

where l is a decay length and V_0 is an energy which depends on the z origin and is hence irrelevant in terms of the scattering power of the potential. The periodic height function h has the Fourier series expansion

$$h(x,y)=\sum_{m,n} d_{mn}\exp[2\pi i(mx+ny)/a]\ , \tag{2}$$

where a is the lattice constant of the substrate surface net. The exponential form is not exact, so the height coefficients d_{mn} will vary slowly with the charge-density value we choose to fit. Fitting at $\rho=6\times10^{-5}$, we find $l=0.65$, $d_{1/2,1/2}=0.26$, $d_{11}=-0.05$ for the SOM, and $l=0.68$, $d_{1/2,1/2}=0.012$, $d_{10}=0.036$ for the MLM. l and d are in a.u., with phases based on an origin at the surface Cl, symmetry-equivalent d's have the same value, and other coefficients are in the noise.

II. EXPERIMENTAL

A. Apparatus

The apparatus used in these experiments has been slightly modified from that described previously.[11] It consists of a He nozzle source of orifice $d_N=5\times10^{-3}$ cm, which is operated at room temperature or $T_N\sim100$ K with a driving pressure typically $P_0=5\times10^3$ Torr. The He beam passes through a skimmer of 1.8×10^{-2} cm diam into a second differentially pumped chamber where it is square-wave chopped at ~200 Hz. It is then collimated to $\sim0.2°$ (in the scattering plane) by a rectangular aperture (0.064×0.2 cm) before entering the ultrahigh-vacuum (UHV) scattering chamber and impinging on the crystal sample. The nozzle-to-crystal distance is 36 cm. The quadrupole mass spectrometer detector (12.5 cm from the sample) is differentially pumped and double collimated. The collimating aperture nearest the sample ($d_1=4$ cm) has a diameter of 0.037 cm, which determines the circular area on the sample viewed from the ionizer with an angular width of 0.3°. The collimator nearer the ionizer ($d_2=10$ cm) determines the in-plane acceptance angle for a point source on the sample, which is also 0.3°. The lateral spread of the incident beam for this configuration, however, results in an apparent angular width of $\sim1°$ which sets the limit to which we can determine scattered beam widths.

The He signal was collected in analog form using a lock-in amplifier set at the phase of the elastic scattering signal. The incident and scattered angles were determined by the settings of the detector for the straight-through beam and the specular beam. These were set to 0.1° with an accuracy of 0.2°. The sample was aligned approximately in plane using the specular beam and then refined by tuning the azimuth angle and sample tilts to maximize the in-plane diffraction beams far from specular. Strong bound-state resonances rendered the use of just the specular beam insufficient for adequate alignment.

The He-beam wavelengths were $\lambda=0.57$ Å ($T_N=300$ K), $\lambda=0.80$ Å ($T_N=130$ K), and $\lambda=0.94°$ Å ($T_N=110$ K). The full width at half maximum (FWHM) wavelength distribution values were $(\Delta\lambda/\lambda)\sim8\%$ (0.57 Å) and 3% (0.8 Å and 0.9 Å). Some of the data were taken after the collimating apertures were changed to what we will term low resolution. Pertinent parameters for these observations were the following: The incident beam divergence was 0.43°, the nominal detector angular resolution was 1.4°, and the chopping frequency was 800 Hz. With allowance for the change in resolution, these later results reproduced those found earlier. Data taken with this configuration will be explicitly denoted in the text.

B. Ag{001} sample

1. Sample preparation

The square Ag{001} sample with dimensions (mm^3) $11\times11\times1$ was cut from a single-crystal boule of 99.999% purity. The surface was oriented within 0.5° of the (001) plane and polished with alumina grit of successively smaller sizes, ending with 0.3 μm. It was then electropolished in the solution $KCN:Na_2CO_3:H_2O$ in a ratio of 1:1:22 using a Ta cathode at about 5 V and 1.5 A for 15 sec. This removes mechanical strains but leaves a nonuniform visual appearance which for our crystals persisted through extensive sputtering and annealing. Approximately 40 h of sputtering with Ar^+ at room temperature at 1 kV and 5 μA, with interspersed anneals at 600 K were required to produce a surface showing only Ag in the Auger electron spectroscopy (AES) spectrum. A weak broad peak consistently appearing near 510 eV was attributed to silver rather than to oxygen. For a newly sputtered and annealed surface, the AES ratio [C + Ag(265)/Ag(304)] was 0.43 ± 0.02. From the consistency of this ratio after extensive sputtering, and the lack of apparent broadening of the peak near 265 eV, we conclude that the surface carbon contamination was negligible.[12]

The sample was held against the end of a Ta cylinder by spot-welded Ag wires. It could be heated from the rear by radiation from a tungsten filament or cooled to ~130 K by conduction from a flexible copper strap connected to a liquid-nitrogen reservoir. A chromel-alumel thermocouple was spot welded to the edge of the sample.

2. Sample surface characterization

The structure of the Ag{001} surface was examined using He-atom diffraction and LEED. Two areas of the surface were identified which produced different widths of the He scattered beams. Both produced visually sharp

LEED patterns with low background. We worked with the smaller area of the sample which produced a specular He beam narrower than our detector angular resolution (FWHM=1°). Over the rest of the sample (major portion), the He specular beam width was 1.6° indicating a lower degree of long-range order. For the small area at $T_s=300$ K, the in-plane integrated specular intensity at $\theta_i=60°$ amounted to 25% of the incident beam indicating a smooth surface at the atomic level.

C. Chlorination

The corrosive properties of chlorine require a procedure which minimizes the chlorine exposure of the system. In early experiments, chlorine gas was fed directly into the nozzle directed at the sample. The sample chamber pressure did not exceed 2×10^{-9} Torr. This procedure worked satisfactorily and the $c(2\times2)$ pattern was produced with the sample at temperatures in the range 270—500 K. Subsequently a glass capillary-array doser was introduced into the UHV scattering chamber at a distance of 20 cm from the sample. The array, which is 8 mm in diameter, produced a beam at the sample distance with a FWHM of 5°, so that the effective Cl_2 pressure at the sample face was about 4 times that due to the rise in the ambient Cl_2 pressure. In a typical exposure, the Cl_2 pressure behind the array was raised to 1×10^{-4} Torr, and the Cl_2 pressure in the sample chamber was increased to 3×10^{-7} Torr for a period of 3 min corresponding to a dose of 270 L (1 L=1 langmuir=10^{-6} Torr sec). The LEED spectra for the surface structure Ag{001}-$c(2\times2)$Cl thus produced showed no qualitative dependence on the method of preparation or sample temperature in the range 130—400 K.

This procedure for generating the $c(2\times2)$Cl structure is similar to that used in the photoemission experiments by Weeks and Rowe.[2] In the LEED study the Cl structure was generated by decomposition of $C_2H_4Cl_2$ at the Ag surface at elevated temperature ($T_s>400$ K). We show below, however, that the $c(2\times2)$Cl structure we observe is the same as that in the LEED experiment and that it is not sensitive to preparation conditions. Thus we can conclude that the different chlorination procedures are not the source of the apparent disagreement between the photoemission and LEED results.

D. Structure characterization

The $c(2\times2)$Cl structure was characterized by AES, LEED, and He-atom diffraction. The Cl-to-Ag AES peak ratio [Cl(181 K) to Ag(356 K)] was 0.33 ± 0.03. The LEED pattern showed the $c(2\times2)$ symmetry, with qualitatively sharp spots and low background. A visual scan of the LEED beams (I-V spectra) at normal incidence was compared to the published curves of Zanazzi *et al.*[1] Particular attention was paid to the spectral regions where the calculated LEED spectra for the SOM and MLM structures showed significant disagreement. Good agreement was found with the earlier LEED data except for a uniform displacement of all features by about 5 V. As in the previous study, the extrema we observed in the I-V spectra compared more favorably with the calculation for the SOM than the MLM structure in two regions we could identify at normal incidence. We conclude that we had the same structure as that previously studied with LEED. The present LEED I-V spectra were observed to remain qualitatively the same for periods of days and did not depend on sample temperature during or after preparation in the range 150—425 K.

Observations with He-atom diffraction, AES, and LEED also support the conclusion that this $c(2\times2)$Cl surface structure was a stable and unique ordered surface. Details of He diffraction patterns were reproduced after many cycles of sputtering, annealing, and reexposure to Cl_2. The specular He peak from the $c(2\times2)$ structure was found to have the same amplitude within 5% for greatly increased times of Cl_2 exposure. Stability as a function of temperature was checked by heating and monitoring the AES spectrum, LEED, and He diffraction patterns (see below). Although heating to 820 K for ~4 min removed the Cl peak in the AES spectrum, heating at 620 K for several minutes did not. During this lower heating the $c(2\times2)$ LEED pattern was maintained with the same visual I-V extrema positions, but with smaller amplitudes and an increase in the diffuse background. At room temperature and at 1×10^{-9} Torr, no changes in the visual LEED pattern could be detected over a period of 10 days. During this same period, AES peak ratios changed by at most 10%. For a freshly prepared overlayer, the atom diffraction intensities remained essentially constant for a period greater than an hour, and none of the beams decreased by more than 10% in 24 h.

If the sample was held below ~180 K, a rapid decrease in He diffraction peak amplitudes with time (10—15 min) was observed. The intensities could be restored by heating briefly above 180 K. We assume this is due to the reversible adsorption of a background gas. Most of the diffraction data we report have been taken with the sample held at 205 K, at which temperature the surface was stable with time. We did not examine surface structures prepared with Cl_2 exposures less than several langmuirs.

Kitson and Lambert[4] reported that the $c(2\times2)$Cl structure, prepared at 300 K, undergoes an irreversible transition upon heating to $T_s>430$ K for 5 min. They characterized this transition by noting the onset of a relatively high ESD cross section and a deterioration in the sharpness of the LEED pattern which they describe in terms of a Debye-Waller factor. We have looked for changes in the He diffraction pattern after heating the surface to temperatures as high as 650 K, as shown in Fig. 3. At this temperature a large fraction of the adsorbed Cl leaves the surface within 5 min. We discuss the structural implications of these results in a later section. At this point it is sufficient to note that the angular distribution of diffracted intensities is directly related to the structure within the unit mesh. We do not find any changes in the angular distribution of the diffracted beams indicating that a structural change has occurred. Even after heating to 650 K and substantially reducing the surface Cl coverage, the He diffraction pattern retains approximately the same relative angular distribution but with reduced intensities. This indicates that the remaining Cl at lower coverage is still maintaining some $c(2\times2)$ order and with no change in structure within the unit mesh.

E. Diffraction scans

Plots of the reduced scattered beam intensity as a function of scattering angle in the plane of incidence are

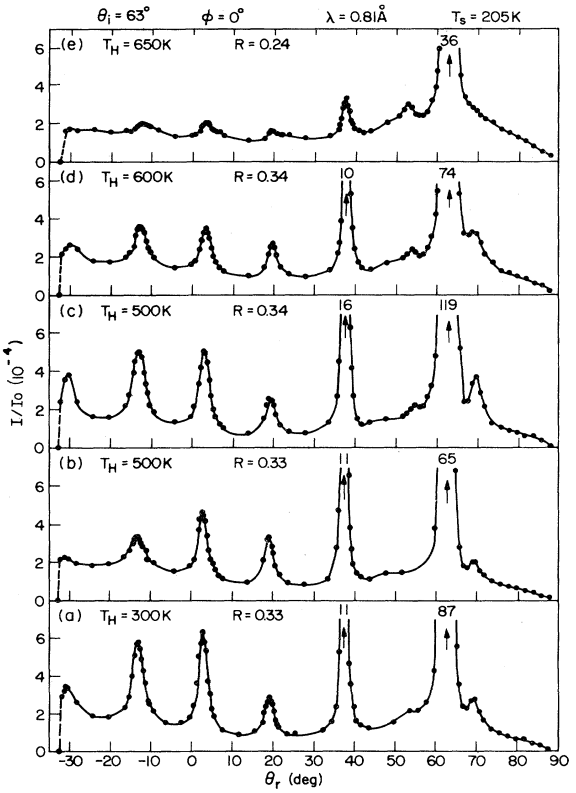

FIG. 3. Series of diffraction scans in the time sequence (a) to (e). Scan (a) was taken 23 h after the Ag{001}-$c(2\times2)$Cl structure was prepared at ~300 K by exposure to Cl_2. After the exposure, the surface was examined by LEED and AES, with the AES peak-to-peak ratio R[Cl(181 K) to Ag(356 K)]=0.33. After scan (a) was taken, the sample was held at 460 K for 5 min, and cooled again to 250 K for a diffraction scan. It was then heated to 500 K for 5 min, and cooled to 250 K for another diffraction scan, shown in (b). The scan after heating at 460 K was identical with (b). The sample was then kept in the ambient vacuum at 300 K at a pressure of 7×10^{-10} Torr for 45 h. The AES ratio R was found to be unchanged at 0.34, and scan (c) was taken. Scans (d) and (e) were then taken in quick succession, each after a 5-min heat at the temperature shown. Observe that the peak in the envelope of the diffraction beams near $\theta_r=-3°$ remains fixed through the series, even when the peaks are becoming smaller and the chlorine concentration is decreasing.

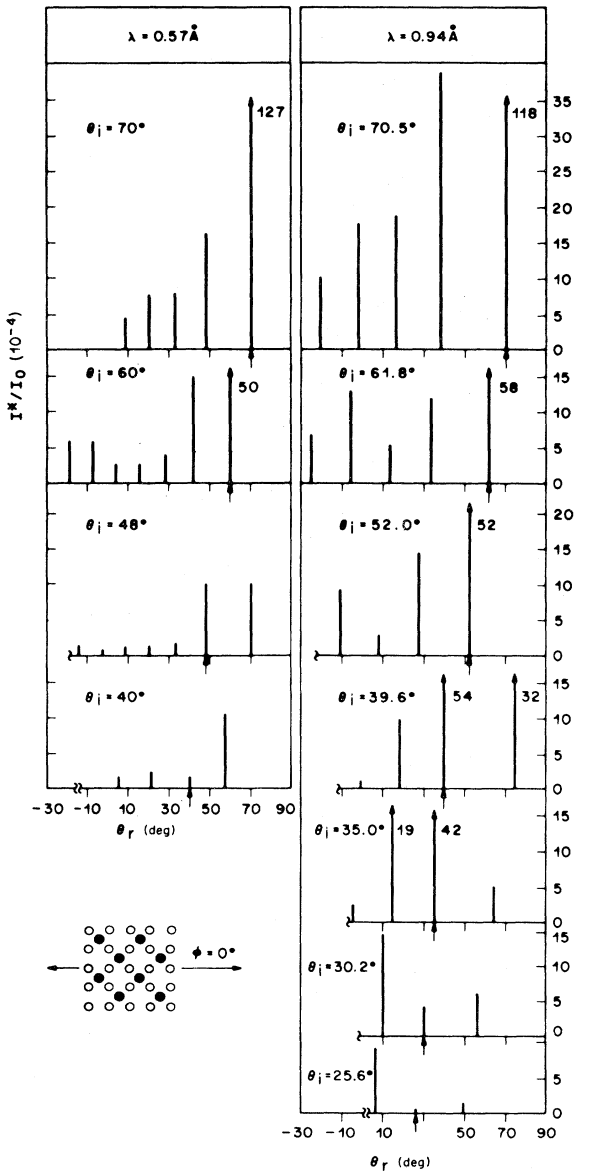

FIG. 4. Series of diffraction scans at two wavelengths, azimuth 0°, and several angles of incidence, for He atoms on Ag{001}-$c(2\times2)$Cl. Sample temperature was 250 K. Diffraction peak intensities have been normalized as specified in the text.

shown in Figs. 4 and 5. Diffraction peaks appear at the angles satisfying the grating formula $n\lambda=d(\sin\theta_r-\sin\theta_i)$, where λ has been determined by time-of-flight measurement and d is the appropriate lattice spacing for the given azimuth in the $c(2\times2)$ structure, based on the bulk Ag spacing of 4.086 Å. Once reproducible conditions are established, we fit a more precise value of λ using the positions of the diffraction beams. The widths of the peaks increase as the order of diffraction increases except for the beams nearest the specular as is consistent with the velocity spread in the incident beam and the angular acceptance of the detector.

In order to make a quantitative comparison of the experimental data with theory, diffraction probabilities are desirable. In the absence of a computer simulation of all the broadening factors involved, these absolute probabilities cannot be accurately determined. The relative diffraction probabilities, however, are quite accurate. We report the results as

$$\frac{I^*}{I_0}=\left[\frac{\int I_{ij}(\theta)d\theta}{\int I_0(\theta)d\theta}\right]\frac{\cos\theta_r}{\cos\theta_i}\ . \tag{3}$$

The last term accounts for the angle dependence of the incident flux on the variable area viewed by the detector. A

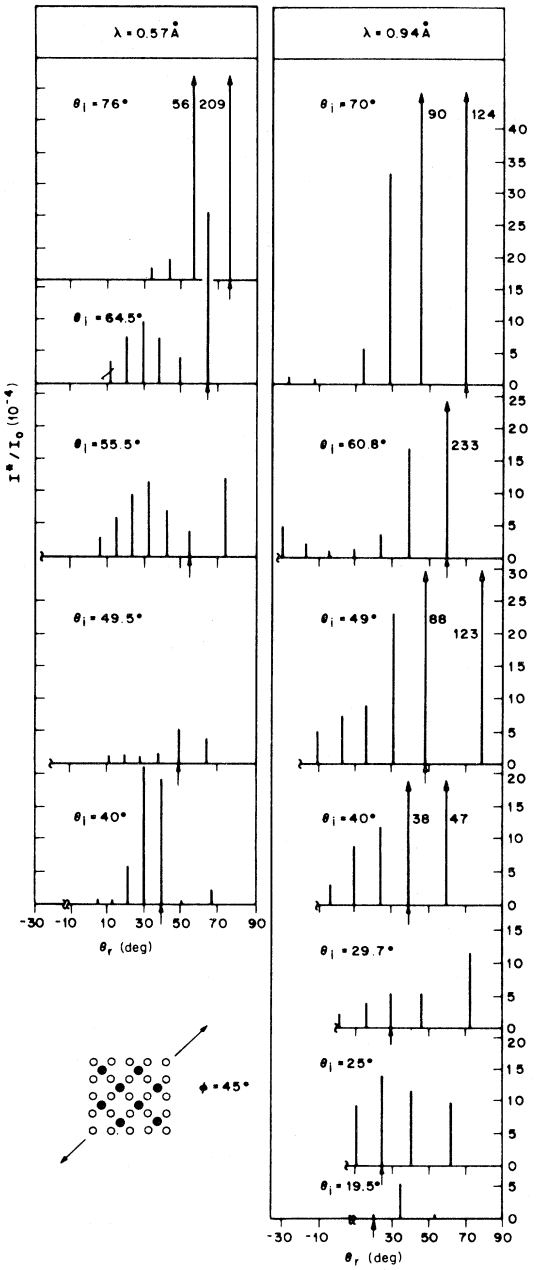

FIG. 5. As for Fig. 4, with azimuth 45°.

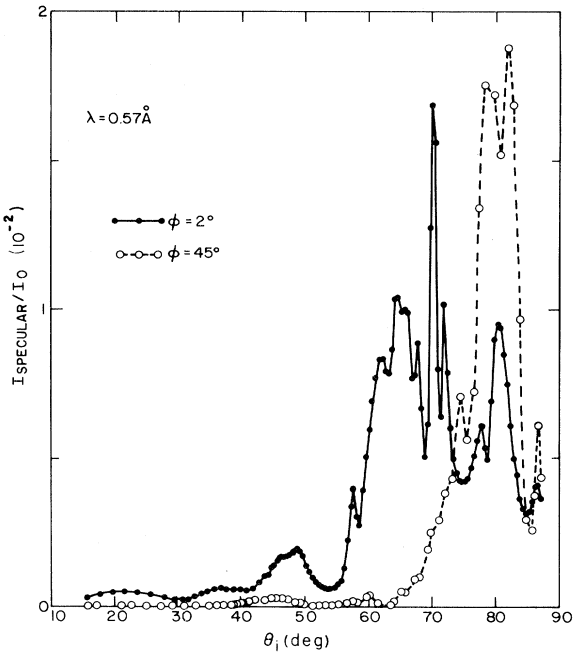

FIG. 6. Plots of the normalized specular intensity as a function of angle of incidence, for He atoms on Ag{001}-$c(2\times2)$Cl, for two azimuths, for $\lambda=0.57$ Å.

smooth background has been subtracted from the diffraction scans. It has been drawn so that the net diffraction peaks have their appropriate widths calculated from the velocity spread and detector acceptance angle.

F. Specular intensity scans

In Figs. 6 and 7 we plot results for selected scans of the specular intensity versus polar angle, θ_i, for two wavelengths and two azimuthal orientations. These data were taken under the conditions termed low angular resolution. A reproducibility check for $\lambda=0.57, \phi=0°$ (high angular resolution), taken months earlier, yielded detailed quantitative agreement upon proper scaling. The azimuths for these scans have been set by alignment of the crystal along symmetry directions by maximizing the intensities of diffraction beams far from the specular.

The sharp oscillatory features of the data are attributable to bound-state resonances associated with the attractive part of the He-surface potential. The assignment of the bound-state energy levels based on the analysis of an extensive set of specular scattering data is the subject of another paper.[13] For the purpose of this work we focus on the envelope of these curves as they are characteristic of the gross corrugated structure of the surface. In the vicinity of any symmetry direction, all the scans taken showed similar envelopes. The azimuths we present here were selected so as to show the common envelope features most clearly.

III. ANALYSIS AND DISCUSSION

A. Estimate of the corrugation

All of the He diffraction data shown in Figs. 3–7 are consistent with a scattering potential corrugation of ~1 Å as expected for the SOM. In particular we focus on Figs. 3–5 where we note that for the scans at $\lambda=0.8$ Å, $\theta_i=63°$, $\lambda=0.94$ Å, $\theta_i=61.8°$, and $\theta_i=52°$, and $\lambda=0.57$ Å, $\theta_i=60°$, maxima may be observed in the envelope of diffracted intensities which are displaced in angle $\Delta\theta_{rb}\sim70°$ from specular. These are rainbow maxima. From either classical or semiclassical scattering theory they can be shown to originate from impact parameters at

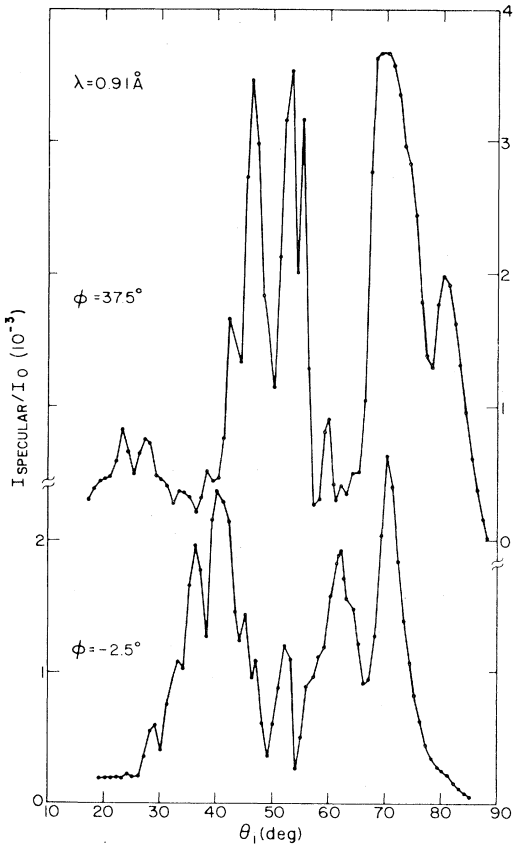

FIG. 7. Plots of the normalized specular intensity as a function of the angle of incidence for two azimuths, for $\lambda=0.91$ Å.

the point of inflection in the scattering potential. This can be illustrated in one dimension with a simple specular scattering function, $f(x)$, over a unit mesh of length L, which is described by one Fourier coefficient

$$f(x)=a\cos\frac{2\pi x}{L} . \tag{4}$$

The differential cross section is proportional to $1/f'(x)$.[14] At the rainbow maximum, $f''(L/4)=0$, which results in a classical singularity. The inclusion of the wave nature of the scattering converts this into a broader maximum at approximately the same angle for sufficiently high energy. The slope, $f'(L/4)$, and the displacement angle of the rainbow maximum from specular, $\Delta\theta_{\rm rb}$, are simply related by

$$f'\left[\frac{L}{4}\right]=\left[\frac{2\pi a}{L}\right]=\tan\frac{\Delta\theta_{\rm rb}}{2} . \tag{5}$$

Thus the corrugation $\zeta=2a$ can be obtained from the deflection angle of the rainbow maximum from specular via

$$\zeta=\frac{L}{\pi}\tan\left[\frac{\Delta\theta_{\rm rb}}{2}\right] . \tag{6}$$

This one-dimensional analysis can be useful in obtaining an estimate of the corrugation along an azimuth where the rainbow can be clearly identified. From Eq. 6 we obtain, for the $\phi=0°$ direction with the separation between the Cl as $L=5.78$ Å and $\Delta\theta_{\rm rb}=-70°$, a corrugation of $\zeta\sim1.3$ Å.

An approximate correction for the effect of the attractive potential of depth D can be included. Using Snell's law of refraction and labeling the angle (θ') and wavelength (λ') within the range of the attractive potential, the changes in angle and wavelength upon refraction become

$$\sin\theta'=\sin\theta[1+D/E]^{-1/2} , \tag{7}$$

$$\lambda'=\lambda[1+D/E]^{-1/2} . \tag{8}$$

We take the value $D=18$ meV from analysis of the He scattering resonances.[13] The inclusion of refraction in this manner leads to a 20% reduction in the estimate for the corrugation along the $\phi=0$ direction, i.e., $\zeta\sim0.9-1.1$ Å, with the larger value associated with the higher energy scattering, $E_i=63$ meV.

Quantum corrections shift the position of the rainbow maximum of the envelope of the diffracted beams closer to the specular direction in the He energy range of interest. This correction can be found to an adequate approximation by solving the relation[15]

$$\sin(t-\Delta\theta_{\rm rb}/2)=0.509(\lambda/L)^{2/3}\cos t\,(\sin t)^{1/3} \tag{9}$$

iteratively for t, and the corrugation height is

$$\zeta=(L/\pi)\tan t . \tag{10}$$

In this short-wavelength limit, the right side of Eq. (9) is zero, and Eq. (10) reduces to the classical result, Eq. (6). Calculating this correction, which should be applied inside the attractive well using the refraction and acceleration corrections given in Eqs. (7) and (8), yields an increase in the estimated corrugation height to $\zeta=1.1-1.3$ Å.

All the above analysis is based on a one-dimensional "slice" of a He-surface potential which is equally corrugated in two directions. To test the validity of this approach, the corrugated exponential wall derived from the electron charge density in Sec. I was used in a complete solution of the quantum-mechanical diffraction problem based on Laughlin's method.[6] The refraction and acceleration produced by the attractive well were incorporated, but not its shape or backscattering properties. In other words, the calculation was carried out for a He energy of 40 meV equal to the incident energy of 25 meV plus a 15-meV well, external and internal beam angles were related through Eq. (7), and internal beams without enough normal momentum to climb out of the well were discarded. The results for three incident angles at $\phi=0°$ are shown in Fig. 8. A rainbow maximum at $\Delta\theta_{\rm rb}\sim62°$ is clear in the results at $\theta_i=33°$ and $\theta_i=48°$, which begins to collapse towards specular at $\theta_i=60°$. Thus the rainbow features of a full calculation for the realistic repulsive potential are consistent with the one-dimensional semiclassical hard-wall analysis. The rainbow angle is somewhat smaller than the experimental value, and this is most probably due to the omission of a realistic attractive potential. The slope of the attractive potential in the region of classical turning points of the He in the total potential enhances the effective corrugation of the repulsive soft wall.[6] This effect,

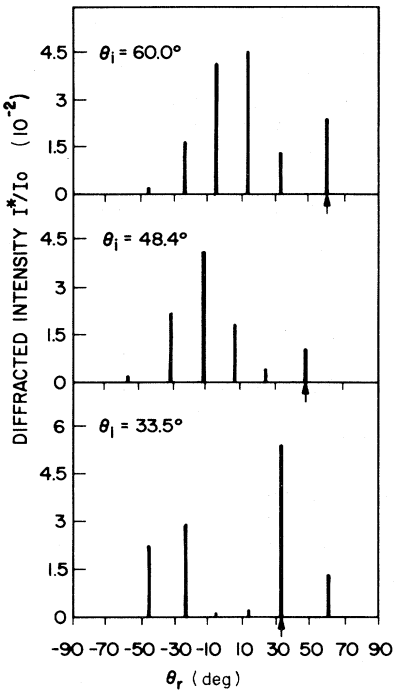

FIG. 8. Theoretical diffraction intensities from a corrugated soft wall for the azimuth $\phi=0°$ and $\lambda=0.91$ Å.

the effect of bound-state resonances on diffraction, and Debye-Waller and other inelastic corrections must all be included before a detailed comparison of theoretical and experimental diffraction intensities can be achieved.

Other characteristics of a strongly corrugated scattering surface can also be identified in the data. A second maximum or supernumerary rainbow evolves out of the specular beam as the incident beam approaches the surface normal, ($\theta_i \lesssim 35°$) for both the $\phi=0°$ and $\phi=45°$ directions, and interference oscillations are observed in the envelope of the specular intensity scans as in Figs. 6 and 7. These two phenomena are closely related and result from the path-length differences upon scattering within a single unit mesh. The specular beam is dominated by the horizontal parts of the unit mesh potential. Qualitatively the oscillations may be considered as resulting from Bragg-type interference in $k_\perp=(2\pi/\lambda)\cos\theta_i$ with maxima located according to the relation

$$2d_\perp\cos\theta_i = n\lambda \ , \tag{11}$$

where $d_\perp$ can be identified with ζ. A similar result comes from the eikonal scattered-wave approximation[16] for which the specular beam intensity is given by $|J_0(c)|^4$. The argument of the Bessel function J_0 is $c=\zeta k\cos\theta$. A tabulation of the maxima in $|J_0|^4$ gives specular interference extrema located almost identically to Eq. (11).

These simple analyses of the interference envelopes in the specular intensity can provide useful information about the corrugation of the scattering potential as recently shown for the semiconductor surfaces.[17] To illustrate the significance of these envelopes in terms of the corrugation, we have listed in Table I a series of angles by which we approximately locate interference maxima in the specular scans of Figs. 6 and 7. To determine the values of $d_\perp$ we have adjusted θ_i and λ_i using the refraction formulas of Eqs. (7) and (8) and assigned diffraction orders to the maxima. The resulting values $d_\perp=1.15$, 0.50, and 0.55 Å, are postulated to be the vertical spacings of the flat regions of the surface which give rise to interference in the specular beam. Based on the surface symmetry they correspond to the sites (a) directly over the Cl atom, (b) the saddle point between adatoms along $\phi=45°$, and (c) directly over the unoccupied fourfold site along $\phi=0°$. This illustration is intended as a qualitative indication of the corrugation. An alternative assignment can be made based on the distances 0.9, 0.5, and 0.4 Å, which similarly accounts based for the positions of the interference features. Regardless of the quantitative accuracy, however, we can conclude that both the diffraction scans and specular interference spectra are characteristic of a surface with a maximum corrugation of 1.0 ± 0.2 Å and therefore in good agreement with the repulsive-potential corrugation based on the charge densities for the SOM.

An important feature of all of these specular scans is that the value of I/I_0 attained at the diffraction minima is nearly zero. This can only occur if the entire surface consists of one structure, the SOM, and eliminates the possibility of the coexistence of both the smooth MLM along with the SOM. The presence of an appreciable fraction of the MLM would keep the specular intensity from dropping to a value near zero as there would always be a fraction of the incident beam which scattered specularly from the MLM except for coincidental resonance minima for both surfaces.

B. Comparison with GaAs(110)

An interesting comparison can be made with certain features of the diffraction and specular intensity scans of the Ag{001}-$c(2\times2)$Cl surface and those of the GaAs{110} surface[17(a)] as shown in Figs. 9 and 10. For both the GaAs{110} potential in the long direction of the rectangular unit mesh ($L=5.65$ Å) [Ref. 17(a)] and the one-dimensional potential "slice" through the Cl's in the

TABLE I. The assignment of interference features of specular intensity scans for the two wavelengths λ employed. Listed are the azimuth ϕ, specular polar angle θ_i, assigned order of diffraction maximum n, and distance $d_\perp$ corresponding to the Bragg-type maximum.

λ (Å)	ϕ	θ_i	n	$d_\perp$
0.91	−2.5°	40	1	0.50
0.91	−2.5°	63	1	0.60
0.91	−2.5°	78	2	1.20
0.91	37.5°	25	3	1.20
0.91	37.5°	50	1	0.55
0.91	37.5°	70	2	1.15
0.57	2°	22	4	1.15
0.57	2°	37	2	0.65
0.57	2°	47	3	1.10
0.57	2°	65	1	0.50
0.57	2°	80	1	0.65

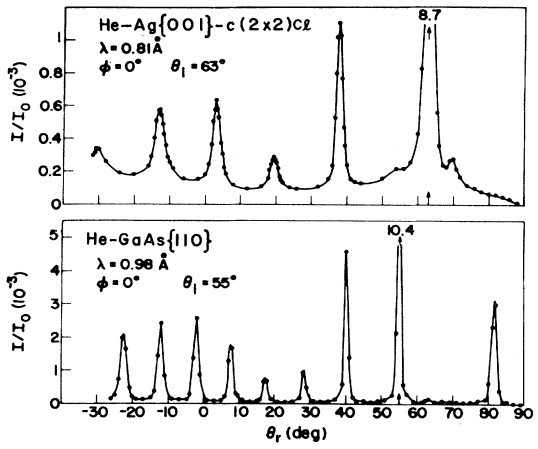

FIG. 9. Diffraction scans for two systems: upper curve, He—Ag{001}-$c(2\times2)$Cl; lower curve, He—GaAs{110}. The angular resolution was significantly better for the lower curve.

$\phi=0°$ direction of the SOM ($L=5.78$ Å), the peak-to-peak corrugation is ~1 Å. In Fig. 9 it can be observed that $\Delta\theta_{rb}$ is approximately the same for both cases. The smaller number of beams in the Ag{001}-$c(2\times2)$Cl scan is due to the two-dimensional symmetry of this surface.

A striking similarity can also be observed in the complex structure of the envelopes of the specular intensity scans at $\lambda=0.57$ Å in Fig. 10. Lower energy scans also show similar overall envelopes characteristic of structural interference despite the different resonance features.

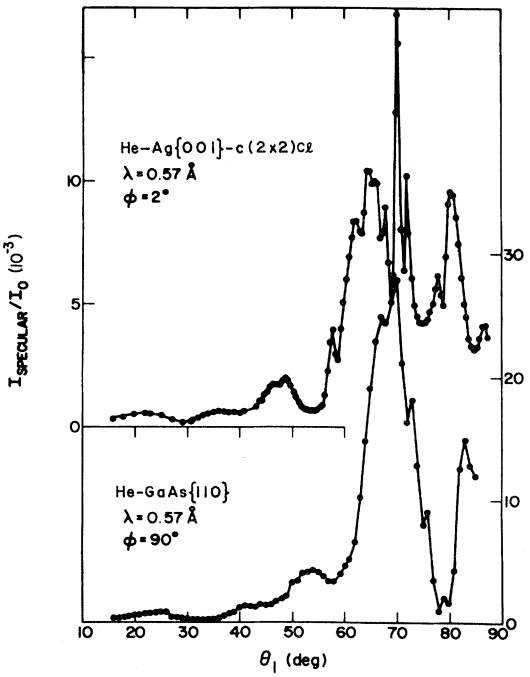

FIG. 10. Plots of normalized specular intensity vs angle of incidence.

This comparison with the well-characterized He-GaAs{110} surface[6,7,17(a)] constitutes strong evidence for the qualitative validity of the one-dimensional and classical arguments employed here which clearly indicate that the SOM, with a maximum corrugation $\zeta\sim1$ Å, is the structure of the $c(2\times2)$Cl overlayer.

C. Requirement for a quantitative fit

The approximate analysis of the previous section is sufficient to unambiguously decide between the SOM and the MLM. In order to proceed to a more quantitative discussion to obtain a value for the Ag—Cl bond length, a considerably greater effort must be expended. A quantitative analysis based on full diffraction calculations must include the attractive part of the He—Ag{001}-$c(2\times2)$Cl potential which is of substantial depth.[13] Preliminary calculations indicate an extreme sensitivity of the calculated diffraction intensities to the details of the scattering potential due to a large extent to the multitude of resonances which occur. A quantitative fit to diffraction intensities for a strongly corrugated surface, which includes the effects of resonances, has yet to be achieved for He diffraction. If, for the Cl overlayer structure, a fit to the data were to be achieved, it would be of interest to consider the sensitivity of this fit to the structure and thus the accuracy required in order to be useful in terms of bond lengths. The peak-to-peak corrugation of the He scattering potential of the $c(2\times2)$Cl SOM structure is ~1.0 Å, whereas the vertical corrugation of the Cl nuclei is ~1.7 Å. As a first guess we assume a linear sensitivity of this corrugation ratio to the structural parameters which implies that the principal Fourier coefficients of the He surface potential must be determined to $\sim5\%$ (~0.05 Å) in order to determine the vertical nuclear spacing to 0.1 Å. Comparable accuracy would be required in the theoretical potential based on the nuclear positions. Note that the required accuracy is in the Fourier coefficients describing the corrugation and not the potential magnitude. It is clear that for useful quantitative fits the He scattering potential must be accurately modeled to include the attractive portion while maintaining a comparably accurate relationship to nuclear positions. In the following paper we report on a general prescription for the complete scattering potential for this surface based on analysis of surface resonances.[13] The objective of this paper, the selection between two structures of the Cl overlayer on the Ag{001} surface, is obtained unambiguously with consideration of just the repulsive potential based on the charge densities.

IV. CONCLUSION

The results of this study demonstrate that analysis of He diffraction, based on recent developments in the theory of the scattering potential, permits decisions between structural models, provided that the associated corrugations are sufficiently different. For the case of the $c(2\times2)$Cl adsorption on Ag{001} the decision between the mixed layer model and the simple overlayer model is straightforward. The repulsive potentials, based on calculated charge densities for the two models, are very different. The MLM appears relatively smooth whereas the SOM has a maximum corrugation of ~1 Å. The He dif-

fraction and specular intensity scans are consistent only with the corrugation of the simple overlayer model. A comparison with the scattering from the GaAs{110} surface, for which the charge density shows comparable corrugations,[7] clearly confirms this conclusion. This result confirms the LEED assignment of the Cl geometry.

The origin of the uncertainty for this structure, based on a theoretical comparison with photoemission data, remains unresolved at this point. The SOM is chemically stable and is a unique $c(2\times2)$ surface. We do not observe a structural change at elevated temperatures as reported by Kitson and Lambert.[4] It is possible that the bond length used in the electronic structure calculations for the SOM was too long, resulting in a distortion of the calculated Cl local density of states. A SOM has recently been confirmed using surface-extended x-ray-absorption fine structure for a very similar system, Cu{001}-$c(2\times2)$Cl, and electronic structure calculations based on this experimental bond length are in excellent agreement with detailed angle-resolved photoemission measurements.[18] If these results are used to define a bonding radius for surface-bonded Cl, a revised SOM geometry for Cl on Ag is suggested with the Cl overlayer 0.38 Å closer to the Ag surface layer. A change of this magnitude could qualitatively change the electronic spectrum. If such a shortening of the Ag—Cl bond length results in a distinguishable change in the He potential corrugation, this can be confirmed with a quantitative fit of the He diffraction using the complete scattering potential.

A second possibility is that Cl may react with Ag to form disordered AgCl in regions of the surface which are not atomically smooth. For the smooth surface we have shown that this reaction does not occur even at elevated temperatures. However, for a surface with a large fraction of "rough" regions, it may be possible to activate a reaction to form disordered AgCl while maintaining some $c(2\times2)$Cl order in the smooth regions. This may be the origin of the "surface transition" observed in Ref. 4 and remains a possibility in the photoemission experiment.

ACKNOWLEDGMENTS

The authors acknowledge helpful discussions with J. E. Rowe and P. H. Schmidt.

---

*Present address: Physics Department, Cornell University, Ithaca, New York, 14853.

[1]E. Zanazzi, F. Jona, D. W. Jepsen, and P. M. Marcus, Phys. Rev. B 14, 432 (1976).

[2](a) S. P. Weeks and J. E. Rowe, J. Vac. Sci. Technol. 16, 470 (1979); (b) S. P. Weeks and J. E. Rowe, Solid State Commun. 27, 885 (1978).

[3]H. S. Greenside and D. R. Hamann, Phys. Rev. B 23, 4879 (1981).

[4]M. Kitson and R. M. Lambert, Surf. Sci. 100, 368 (1980).

[5]N. Esbjerg and J. Norskov, Phys. Rev. Lett. 45, 807 (1980).

[6]R. B. Laughlin, Phys. Rev. B 25, 2222 (1982).

[7]D. R. Hamann, Phys. Rev. Lett. 46, 1227 (1981).

[8]P. C. Hohenberg and W. Kohn, Phys. Rev. 136, B864 (1964); W. Kohn and L. J. Sham, Phys. Rev. 140, A1133 (1965).

[9]D. R. Hamann, L. F. Mattheiss, and H. S. Greenside, Phys. Rev. B 24, 6151 (1981).

[10]O. Jepsen, J. Madsen, and O. K. Andersen, Phys. Rev. B 18, 605 (1978).

[11]M. J. Cardillo, C. S. Y. Ching, E. F. Greene, and G. E. Becker, J. Vac. Sci. Technol. 15, 423 (1978).

[12]S. R. Keleman and I. E. Wachs, Surf. Sci. 97, L370 (1980).

[13]G. E. Becker, M. J. Cardillo, J. A. Serri, D. R. Hamann, following paper, Phys. Rev. B 28, 504 (1983).

[14]E. F. Greene and E. A. Mason, Surf. Sci. 75, 549 (1978).

[15]D. R. Hamann (unpublished).

[16]U. Garibaldi, A. C. Levi. R. Spadacini, and G. E. Tommei, Surf. Sci. 48, 649 (1975).

[17](a) M. J. Cardillo, G. E. Becker, S. J. Sibener, and D. R. Miller, Surf. Sci. 107, 469 (1981); (b) M. J. Cardillo, Phys. Rev. B 23, 4279 (1981).

[18]P. H. Citrin, D. R. Hamann, L. F. Mattheiss, and J. E. Rowe, Phys. Rev. Lett. 49, 1712 (1983).